NASA TECHNICAL NOTE

NASA TN D-5146

c. 1

NASA TN D-5146

TECH LIBRARY KAFB, NM

0131932

LOAN COPY: RETURN TO
AFWL (WLIL-2)
KIRTLAND AFB, N MEX

LAMINAR HEAT-TRANSFER DISTRIBUTIONS FOR A BLUNTED-CONE, CONE-FRUSTUM REENTRY CONFIGURATION AT MACH 10

by J. David Dearing

Langley Research Center
Langley Station, Hampton, Va.

NATIONAL AERONAUTICS AND SPACE ADMINISTRATION • WASHINGTON, D. C. • APRIL 1969

TECH LIBRARY KAFB, NM
0131932

LAMINAR HEAT-TRANSFER DISTRIBUTIONS FOR A BLUNTED-CONE, CONE-FRUSTUM REENTRY CONFIGURATION AT MACH 10

By J. David Dearing

Langley Research Center
Langley Station, Hampton, Va.

NATIONAL AERONAUTICS AND SPACE ADMINISTRATION

For sale by the Clearinghouse for Federal Scientific and Technical Information
Springfield, Virginia 22151 – CFSTI price $3.00

LAMINAR HEAT-TRANSFER DISTRIBUTIONS FOR A BLUNTED-CONE, CONE-FRUSTUM REENTRY CONFIGURATION AT MACH 10

By J. David Dearing
Langley Research Center

SUMMARY

The aerodynamic heating characteristics of a spherically blunted cone, cone-frustum reentry configuration with a hypersonic lift-drag ratio of about 1.5 have been determined at a nominal free-stream Mach number of 10 and at Reynolds numbers based on free-stream conditions and model length of 0.56×10^6, 1.47×10^6, and 2.67×10^6. The measured longitudinal distributions exhibit a small dip, or minimum, in the heating just aft of the blunted nose similar to that exhibited by the pressure distributions of blunted cones. On the windward ray, the heating was unaffected by Reynolds number and increased with angle of attack. The measured heat-transfer distributions indicate a narrow band of locally higher heating associated with the reattachment of vortices near the leeward ray for all angles of attack greater than or equal to the forecone half-angle. This phenomenon appears to be dependent upon Reynolds number as well as angle of attack. The measured base heating rate was less than 0.2 percent of the stagnation-point heating rate.

INTRODUCTION

Several recent design studies sponsored by the Langley Research Center have centered around a spherically blunted cone reentry configuration whose aerodynamic characteristics at Mach 6.9 are reported in reference 1. This configuration, developed for a medium lift-drag ratio of 1.5, has satisfactory stability and control characteristics and is self-trimming at maximum lift-drag ratio about a center of gravity at 61 percent of the length. In the current study, the hypersonic aerodynamic heating characteristics have been determined at Mach 10 for the blunted-cone, cone-frustum reentry configuration. The tests were made in the Langley continuous-flow hypersonic tunnel with zero sideslip and with angles of attack from -20° to $+20^{\circ}$. The free-stream Reynolds numbers based on the 1-foot (0.305-meter) model length of 0.56×10^6, 1.47×10^6, and 2.67×10^6 represent the flight regime prior to, during, and just after the condition of maximum heating, respectively, for a typical reentry trajectory from a near-earth orbit.

SYMBOLS

A,B	coordinates for thermocouple locations on wedge (see fig. 2(b))
c_w	specific heat of wall material
D	diameter of model base (see fig. 2(a))
h	local heat-transfer coefficient, $\frac{q_w}{T_{aw} - T_w}$
L	model length
M	Mach number
p	pressure
q	rate of heat flow per unit area
q_w	rate of heat flow per unit area at wall or model surface
$R_{\infty,L}$	Reynolds number based on free-stream conditions and model length, $\frac{\rho_\infty U_\infty L}{\mu_\infty}$
r	radial distance to thermocouple locations on base plate cover (see fig. 2(b))
T	temperature
T_w	temperature at wall or model surface
t	time
U	velocity
x	longitudinal center-line distance measured from nose
α	angle of attack of center line, positive with nose up (see fig. 2(a))
γ	ratio of specific heats
η	laminar temperature recovery factor (assumed equal to 0.84)

λ_w model wall thickness

μ dynamic viscosity of air

ρ density of air

ρ_w density of model wall material

ϕ angular location of thermocouple on cone and base plate cover (see fig. 2(b))

ψ bluntness ratio, $\frac{\text{radius of nose}}{\text{radius of base}}$

Subscripts:

aw adiabatic wall

l local conditions

o condition at stagnation point

t total

∞ free-stream conditions

APPARATUS AND TEST CONDITIONS

Tests

The tests were conducted in the Mach 10 test section of the Langley continuous-flow hypersonic tunnel. Detailed descriptions of the facility and its operation are given in references 2 and 3. The following table lists the nominal test conditions and the calibrated Mach numbers for the investigation:

p_t		T_t		M_∞	p_∞		T_∞		$R_{\infty,L}$
psia	MN/m^2	^oR	^oK		psia	N/m^2	^oR	^oK	
400	2.76	1777	987	10.16	0.0082	56.65	85.6	47.5	0.56×10^6
1100	7.58	1825	1014	10.23	.0219	150.72	87.2	48.5	1.47
2100	14.47	1874	1041	10.27	.0412	283.93	89.2	49.5	2.67

The free-stream quantities were calculated by using the real-gas relations given in reference 4.

The model injection mechanism described in reference 2 was used to inject the approximately isothermal, cooled model into the test section when hypersonic flow at the desired condition was established. By this method, radiation and surface conduction effects were minimized. When retracted from the flow, the model within the sealed injection box was cooled to a predetermined temperature by internal air jets exhausting through a perforated tube inside the model. The angle of attack was varied from -20° to $+20^{\circ}$ in increments of 5°.

Model

The test model (figs. 1 and 2(a)) consisted of a spherically blunted ($\psi = 0.08$), 15.07° half-angle cone ahead of a cone-frustum with a 11.3° half-angle. The model was 12 inches (30.48 cm) long with the cone, cone-frustum junction at half the length. In this configuration, a wedge was removed from the trailing edge of the cone-frustum (fig. 1) to attain trim at maximum lift-drag ratio.

The cone and cone-frustum were rolled from a 0.030-inch (0.076-cm) inconel sheet, and the spherical nose cap was machined from solid inconel to a thickness of 0.094 inch (0.239 cm) and welded to the forward conical section. The base support plate was covered by a very thin, 0.010-inch (0.025-cm) inconel sheet to measure the very low base heating. The cone, cone-frustum combination, and the base plate cover were attached to the sting-mounted base support plate so as to reduce heat conduction effects.

Instrumentation and Data Reduction

Model surface temperatures were measured by using 67 no. 30 chromel-alumel thermocouples spotwelded to the inside surfaces: 50 along nine equally spaced surface generators from $\phi = 0^{\circ}$ to $\phi = 180^{\circ}$, as shown in figure 2(b); nine on the wedge surface; and the remaining eight on the base plate cover. The output from each thermocouple was recorded on magnetic tape at the rate of 20 points per second with the use of a high-speed analog-to-digital converter and data-recording system. By the transient calorimeter technique, the heat-transfer rate is assumed equal to the rate of heat stored in the surface; thus

$$q = h\left(T_{aw} - T_w\right) = \rho_w \lambda_w c_w \frac{dT_w}{dt}$$

The heat-transfer data were obtained before the surface temperature increased enough for radiation and conduction along the surface to be significant, and no correction has

been made for surface conduction or radiation in the data presented. The derivative in the preceding equation was obtained from a least-squares curve fitted to the data over a time interval of from 1 to 4 seconds, depending upon the local rate of temperature change, and was evaluated at the center of this interval. The density and specific heat of inconel were taken from reference 5. The adiabatic wall temperature at each thermocouple was calculated from the equation

$$\frac{T_{aw}}{T_t} = \frac{T_l}{T_t}\left[1 + \eta\left(\frac{\gamma - 1}{2}\right)M_l^2\right]$$

for a laminar recovery factor η assumed equal to 0.84. The local temperature and Mach number were determined by assuming the air to have expanded from the normal shock pressure to that pressure defined by the tangent-cone approximation. Perfect gas, isentropic, and normal shock relationships, with $\gamma = 1.4$, were used in the calculations.

RESULTS AND DISCUSSION

Heating Distributions

Heat-transfer distributions at a free-stream Mach number of 10.23 and a free-stream Reynolds number based on body length of 1.47×10^6 are shown in figures 3, 4, 5, 6, and 7 for angles of attack of 0°, 5°, $\pm 10^\circ$, 15°, and $\pm 20^\circ$, respectively. In part (a) of each figure, the ratio of local heat-transfer coefficient h to laminar stagnation-point heat-transfer coefficient h_o is plotted as a function of circumferential angle ϕ at five longitudinal stations x/L. In part (b) of each figure, the same ratio of heat-transfer coefficients is plotted as a function of the ratio of longitudinal distance x to model length L at three circumferential locations ($\phi = 0^\circ$, $\phi = 90^\circ$, and $\phi = 180^\circ$). The value of laminar stagnation-point heat-transfer coefficient h_o is given with each figure and was obtained from exact similar solutions as presented in reference 6.

The measured circumferential distributions at $0^\circ < \alpha < 15^\circ$ decrease monotonically from the windward ray ($\phi = 0^\circ$) to the leeward ray ($\phi = 180^\circ$). For $\alpha = 15^\circ$ and $\alpha = \pm 20^\circ$ (figs. 6 and 7, respectively), the heating beyond $\frac{x}{L} = 0.143$ decreased to a minimum at $\phi \cong 160^\circ$ and then increased rapidly toward the leeward ray by as much as a factor of 10. This phenomenon is associated with the separation of vortices from the cone surface near the minimum heating point and reattachment along the leeward ray as observed at lower Mach numbers in reference 7. It should be noted, however, that the leeward heating peak is not present for angles of attack less than the forecone half-angle (15°) except at the most rearward longitudinal stations $\left(\text{i.e., } \frac{x}{L} > 0.8\right)$ at $\alpha = \pm 10^\circ$, the indication being that there is no shedding of vortices at these lower angles of attack.

A series of photographs of the surface flow patterns recorded by oil streaks on the model after a 30-second oil-flow test in the Langley 11-inch hypersonic tunnel at $M_\infty = 6.9$, $R_{\infty,L} = 1.8 \times 10^6$, and $\alpha \cong 15^\circ$ is presented in figure 8. The collection of oil along $\phi \cong 160^\circ$ represents convergence of the flow, which is characteristic of separation, or shedding of a vortex, as depicted in the simplified flow diagram in figure 8. Also, the divergence of the oil streaks near $\phi = 180^\circ$ is indicative of a stagnation-line type of flow created by the mutual action of the counterrotating vortices. Although it is expected that the vortices formed would be weak, transition over the separation region could contribute to the peak observed in the heating data. The location of the minimum in the circumferential heating distribution corresponds closely to the location of the separation line in the oil streaks.

The expected theoretical longitudinal heating distributions for a cone, cone-frustum configuration with no bluntness-induced pressure gradients would consist of a continuous decrease from a high heating level at the nose to a much lower level at the cone, cone-frustum junction, followed by a further decrease as the flow expands around the corner and a final gradual decrease toward the base. However, at $\frac{x}{L} = 0.15$ the measured longitudinal heating distributions (part (b) of figs. 3 to 7) exhibit a small dip, or minimum, which corresponds to the pressure-distribution dip characteristic of blunted cones as shown in references 8 and 9. It appears, therefore, that the heating-distribution dip is the result of bluntness-induced pressure gradients on the blunted cone. Since the level of pressure on the blunted cone to about $\frac{x}{L} = 0.4$ would be lower than expected, the heating would also be somewhat lower.

A comparison of the heat-transfer distributions at equal positive and negative angles of attack (figs. 5 and 7) indicates the good repeatability of the data. Also, figure 3 for $\alpha = 0^\circ$ and figures 5 and 7 for $\alpha = \pm 10^\circ$ and $\alpha = \pm 20^\circ$, respectively, indicate that the flow was symmetrical about the tunnel axis.

Laminar boundary layers would be expected at the Reynolds numbers and Mach numbers of the present tests. In addition, the longitudinal distributions exhibit no large, sudden increases indicative of transition from laminar to turbulent flow. The lack of such an increase in the heating does not, however, totally exclude the possibility of turbulent flow in the vicinity of the leeward vortex action.

At $\frac{x}{L} = 0.5$ the flow expands through 3.8° at the corner junction of the blunted cone and the cone-frustum, resulting in a decrease in the heating by about one-third on the windward ray ($\phi = 0^\circ$) and on the side ray ($\phi = 90^\circ$). (See figs. 3 to 7.) On the leeward ray ($\phi = 180^\circ$), some decrease occurs at the junction for all angles of attack. The leeward-ray distributions for $\alpha \geqq 10^\circ$ exhibit a dip after the expansion and then a rise to the higher local values as discussed previously.

The four data points located from $\frac{x}{L} = 0.9$ to $\frac{x}{L} = 1.0$ on the windward ray represent the heating to the wedge at the base of the aft cone or cone-frustum, which was less than 2.5 percent of the laminar stagnation-point heating at all the test conditions. Similarly, over the entire base plate cover, the heating rates (not presented) were less than 0.2 percent of the stagnation-point heating rate.

In order to obtain an estimate of the magnitude of the heating on a cone, cone-frustum configuration entering the atmosphere from a near-earth orbit, a trajectory was calculated for a vehicle with a lift-drag ratio of 1.42 and a ratio of weight to base area of 160 lb/ft^2 $\left(7.66\ \text{kN/m}^2\right)$. The stagnation-point heating rate q_o on the 0.60-foot-radius (0.183-meter) hemispherical nose for a 30.0-foot-long (9.14-meter) vehicle was found to be 380 Btu/ft^2-sec $\left(4.31\ \text{MW/m}^2\right)$. At a temperature of 3460° R (1922° K), which is approximately the upper limit of most coated refractory metals, a surface with an emissivity of 0.9 will radiate at the rate of 61 Btu/ft^2-sec $\left(692\ \text{kW/m}^2\right)$, which is 16 percent of the stagnation-point heating rate $\left(\frac{q}{q_o} = 0.16\right)$. Now, for comparison with the presented data,

$$\frac{h}{h_o} = \frac{q}{q_o}\left[\frac{1}{\eta}\left(\frac{1 - \frac{T_{w,o}}{T_{aw,o}}}{1 - \frac{T_w}{T_{aw}}}\right)\right]$$

With nonisothermal wall effects neglected, with the assumption that $T_w = 3460^\circ$ R (1922° K) and $\eta = 0.84$, and for hypersonic Mach numbers, $\frac{h}{h_o} \cong 0.2$. Examination of the test results (figs. 3 to 7) reveals that only on the windward surface of the first 10 percent of the body at high angles of attack ($\alpha \geqq 20^\circ$) is this limiting condition exceeded.

Reynolds Number and Angle-of-Attack Effects

The effects of Reynolds number and angle of attack are presented in figures 9 and 10 for three free-stream Reynolds numbers based on body length and three angles of attack. The windward-ray ($\phi = 0^\circ$), longitudinal distributions (fig. 9) indicate no effect of Reynolds number over the test range. The circumferential distributions (fig. 10), however, do exhibit an effect of Reynolds number, predominantly on the most leeward ray ($\phi = 180^\circ$) at angles of attack of 10° and 20°. A smaller effect can be noted as far around as $\phi = 120^\circ$. This effect is not exhibited at zero angle of attack.

On the leeward surfaces, the effect of angle of attack is complex because of the formation of the previously mentioned counterrotating pair of vortices at angles of attack of 10° and greater. The effect of Reynolds number on the formation of these vortices can be observed in figure 10(b) at stations $\frac{x}{L}$ of 0.638 and 0.836. At the lowest

Reynolds number, no peak and possibly no vortices exist, but, at the two higher Reynolds numbers, the increase in heating resulting from the formation of the vortices is present. The heating minimum at $\phi \cong 150^{\circ}$, which is also the apparent vortex separation location, decreases with increasing Reynolds number and angle of attack. Whenever this minimum is followed by a peak heating point at $\phi = 180^{\circ}$, characteristic of the presence of the vortex pair, the peak heating value increases with Reynolds number and angle of attack.

CONCLUSIONS

A spherically blunted cone, cone-frustum reentry configuration has been tested at a nominal free-stream Mach number of 10 and at Reynolds numbers based on free-stream conditions and model length of 0.56×10^6, 1.47×10^6, and 2.67×10^6, representing the flight regime of such a configuration during conditions of maximum heating in a typical reentry trajectory. The measured heating distributions indicate the following results:

1. The circumferential distributions of heating at angles of attack of 15° and greater increase sharply in a very narrow region near the leeward ray as a result of separation of vortices from the surfaces near the leeward ray and reattachment of the flow at the leeward ray.

2. The measured longitudinal heating distributions exhibit a small dip, or minimum, just aft of the blunted nose similar to that observed in pressure distributions for blunted cones.

3. On the windward ray, the heating was unaffected by Reynolds number. Changes in heating near the most leeward ray indicate a vortex dependence upon Reynolds number as well as angle of attack.

4. Heating on the wedge at the base of the cone-frustum was less than 2.5 percent of the laminar stagnation-point heating.

5. The base heating rate was found to be less than 0.2 percent of the stagnation-point heating rate.

Langley Research Center,
National Aeronautics and Space Administration,
Langley Station, Hampton, Va., February 3, 1969,
124-07-02-70-23.

REFERENCES

1. Penland, Jim A.; and Bernot, Peter T.: Aerodynamic Characteristics of Three Axisymmetric Low-Fineness-Ratio Reentry Shapes at Mach 6.9. NASA TN D-4122, 1967.

2. Dunavant, James C.; and Stone, Howard W.: Effect of Roughness on Heat Transfer to Hemisphere Cylinders at Mach Numbers 10.4 and 11.4. NASA TN D-3871, 1967.

3. Hamilton, H. Harris; and Dearing, J. David: Effect of Hinge-Line Bleed on Heat Transfer and Pressure Distribution Over a Wedge-Flap Combination at Mach 10.4. NASA TN D-4686, 1968.

4. Erickson, Wayne D.; and Creekmore, Helen S.: A Study of Equilibrium Real-Gas Effects in Hypersonic Air Nozzles, Including Charts of Thermodynamic Properties for Equilibrium Air. NASA TN D-231, 1960.

5. Lucks, C. F.; and Deem, H. W.: Thermal Properties of Thirteen Metals. Spec. Tech. Publ. No. 227, Amer. Soc. Testing Mater., 1958.

6. Cohen, Nathaniel B.: Boundary-Layer Similar Solutions and Correlation Equations for Laminar Heat-Transfer Distribution in Equilibrium Air at Velocities up to 41,100 Feet Per Second. NASA TR R-118, 1961.

7. Rainbird, W. J.; Crabbe, R. S.; Peake, D. J.; and Meyer, R. F.: Some Examples of Separation in Three-Dimensional Flows. Can. Aeronaut. Space J., vol. 12, no. 10, Dec. 1966, pp. 409-423.

8. Cleary, Joseph W.: Effects of Angle of Attack and Nose Bluntness on the Hypersonic Flow Over Cones. AIAA Paper No. 66-414, June 1966.

9. Cleary, Joseph W.: An Experimental and Theoretical Investigation of the Pressure Distribution and Flow Fields of Blunted Cones at Hypersonic Mach Numbers. NASA TN D-2969, 1965.

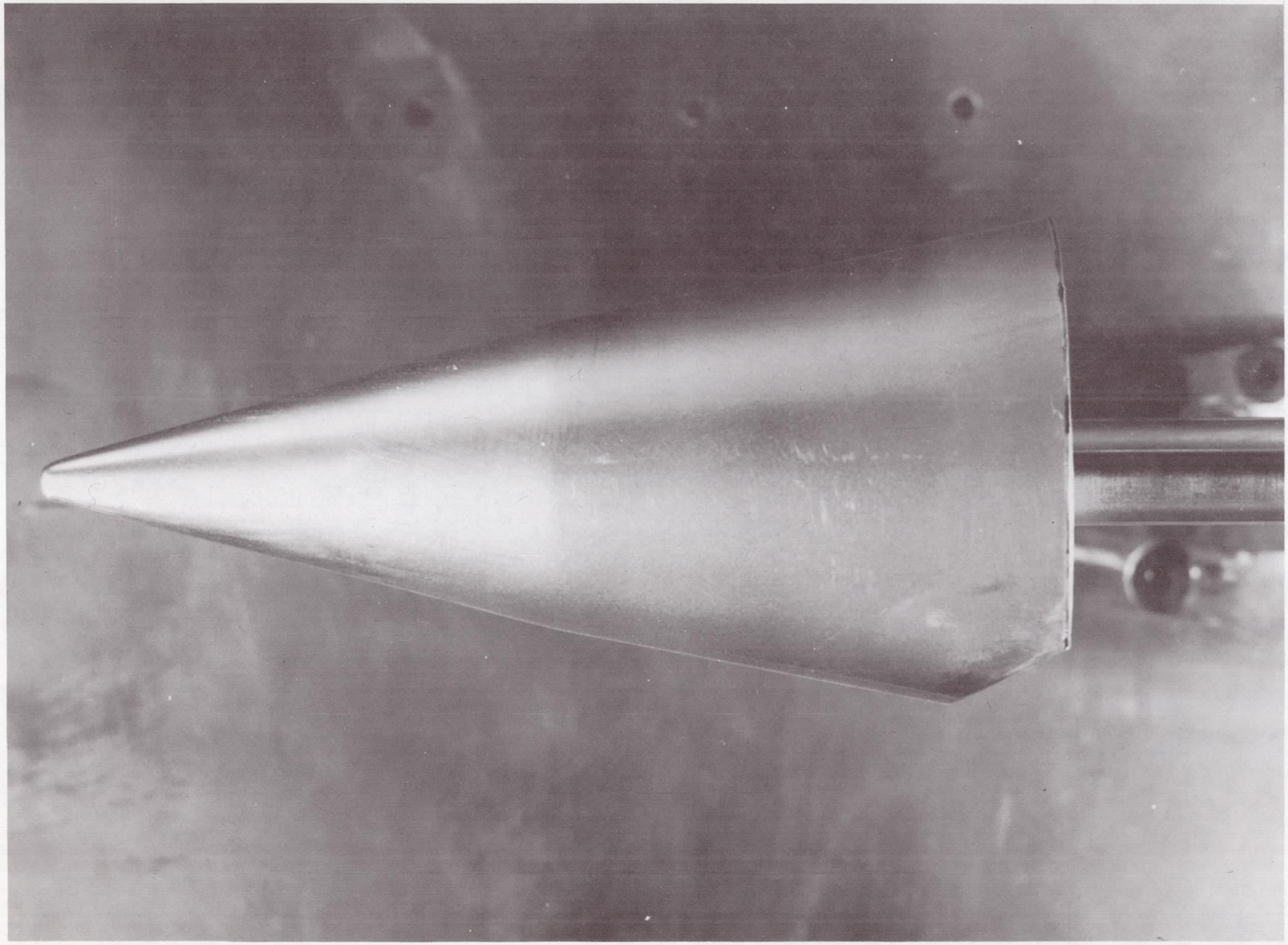

Figure 1.- Side view of the blunted-cone, cone-frustum model.

L-67-7917

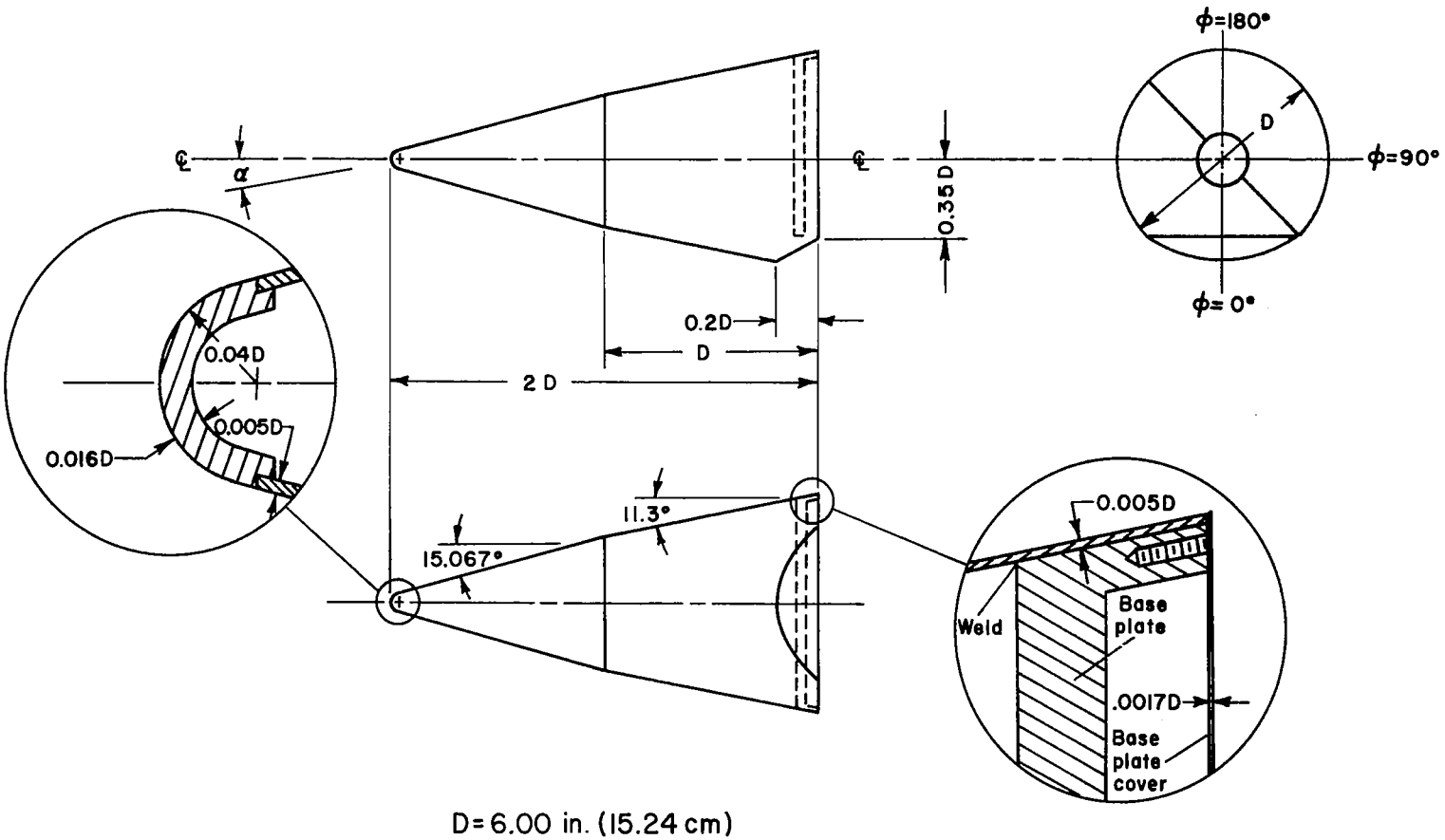

(a) Model geometry.

Figure 2.- Sketches of model.

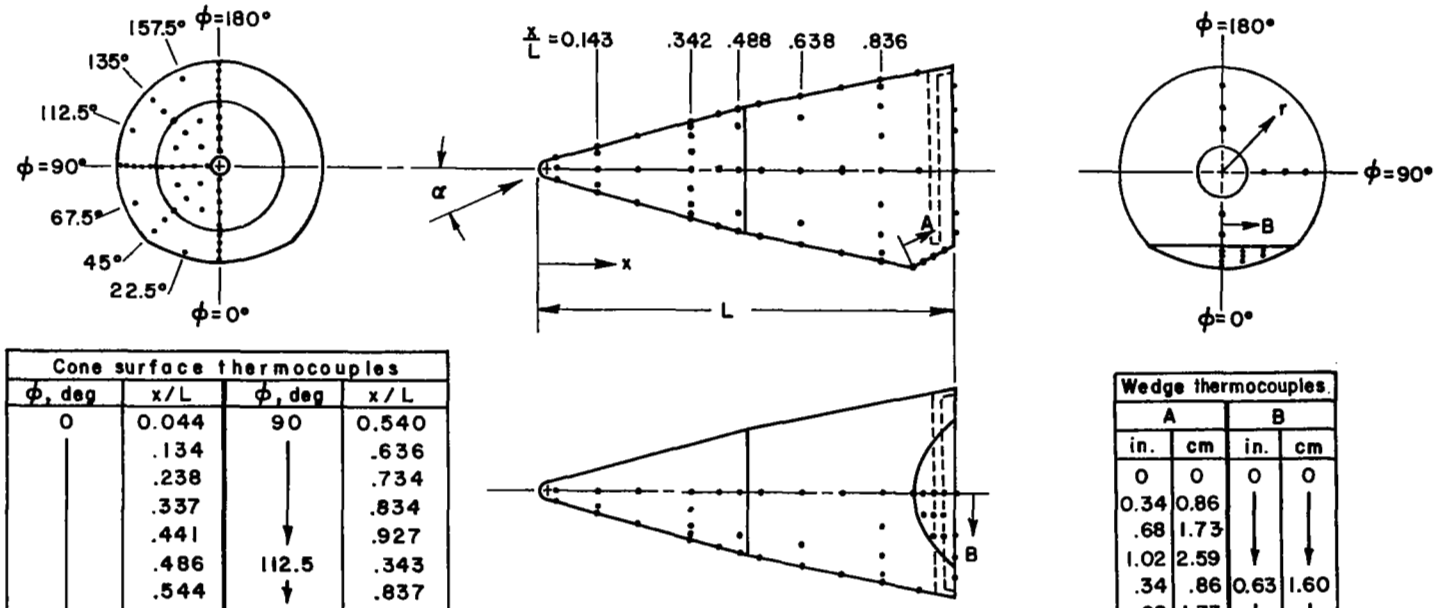

Cone surface thermocouples			
φ, deg	x/L	φ, deg	x/L
0	0.044	90	0.540
	.134		.636
	.238		.734
	.337		.834
	.441		.927
	.486	112.5	.343
	.544		.837
	.636	135	.146
	.737		.348
	.836		.489
22.5	.340		.636
	.839		.837
45	.140	157.5	.346
	.340		.837
	.488	180	.039
	.638		.149
	.835		.243
67.5	.346		.345
	.834		.440
90	.043		.487
	.147		.537
	.244		.643
	.335		.734
	.439		.833
	.491		.927

L = 12.00 in. (30.48 cm)

Wedge thermocouples			
A		B	
in.	cm	in.	cm
0	0	0	0
0.34	0.86		
.68	1.73		
1.02	2.59		
.34	.86	0.63	1.60
.68	1.73		
1.02	2.59		
.68	1.73	1.25	3.18
1.02	2.59		

Base thermocouples		
φ, deg	r	
	in.	cm
0	1.20	3.05
	1.80	4.57
90	1.20	3.05
	1.80	4.57
	2.40	6.10
180	1.20	3.05
	1.80	4.57
	2.40	6.10

(b) Instrumentation details.

Figure 2.- Concluded.

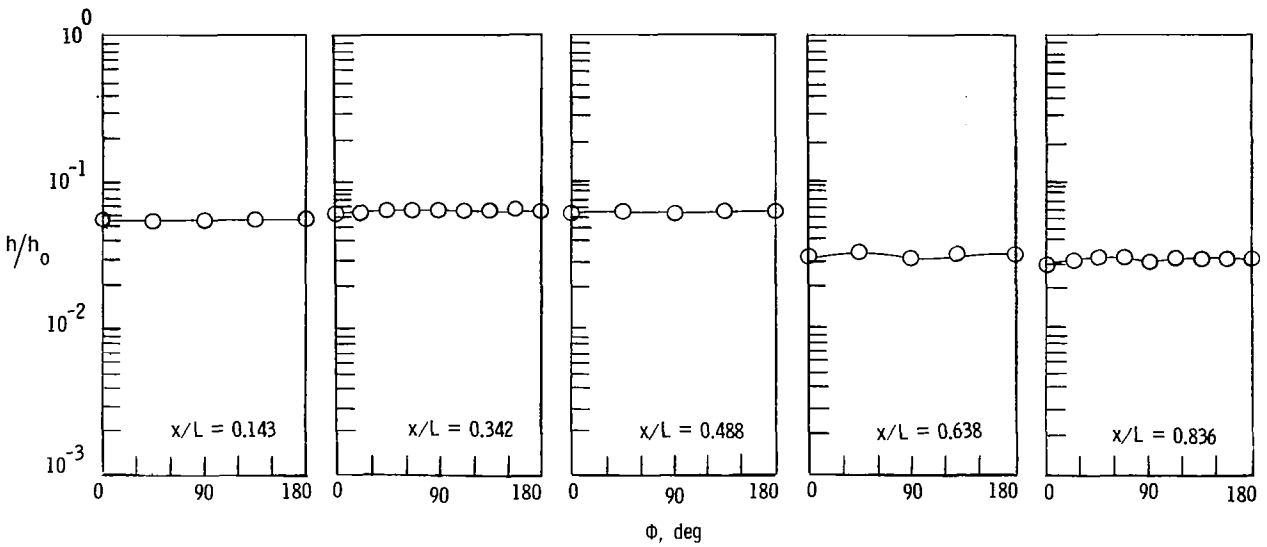

(a) Circumferential distributions.

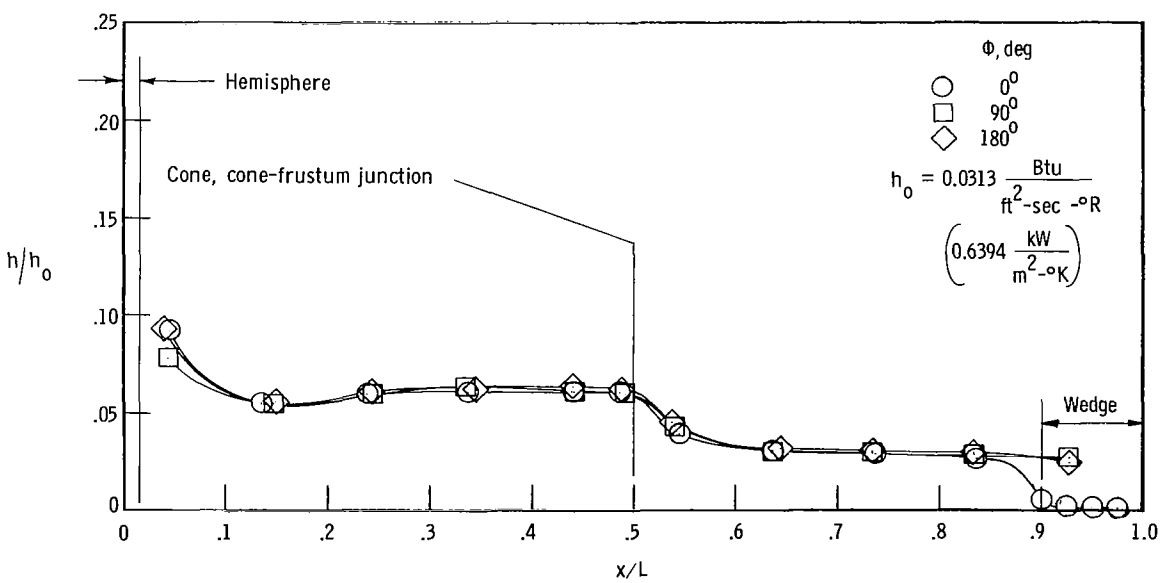

(b) Longitudinal distributions.

Figure 3.- Heat-transfer distributions for cone, cone-frustum configuration at $\alpha = 0^0$, $M_\infty = 10.23$ and $R_{\infty,L} = 1.47 \times 10^6$.

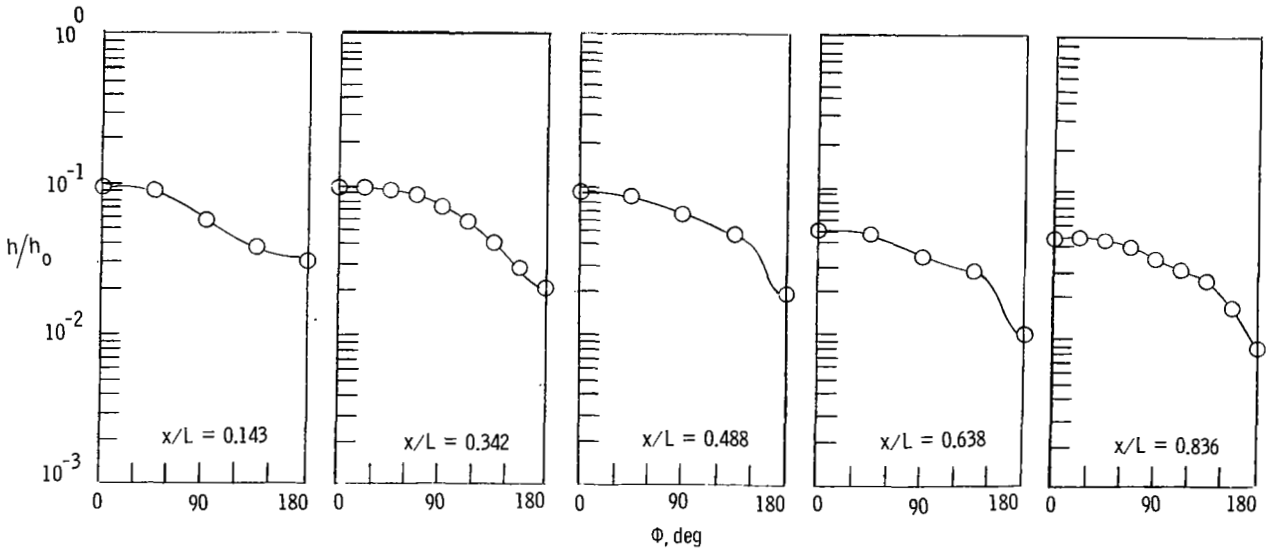

(a) Circumferential distributions.

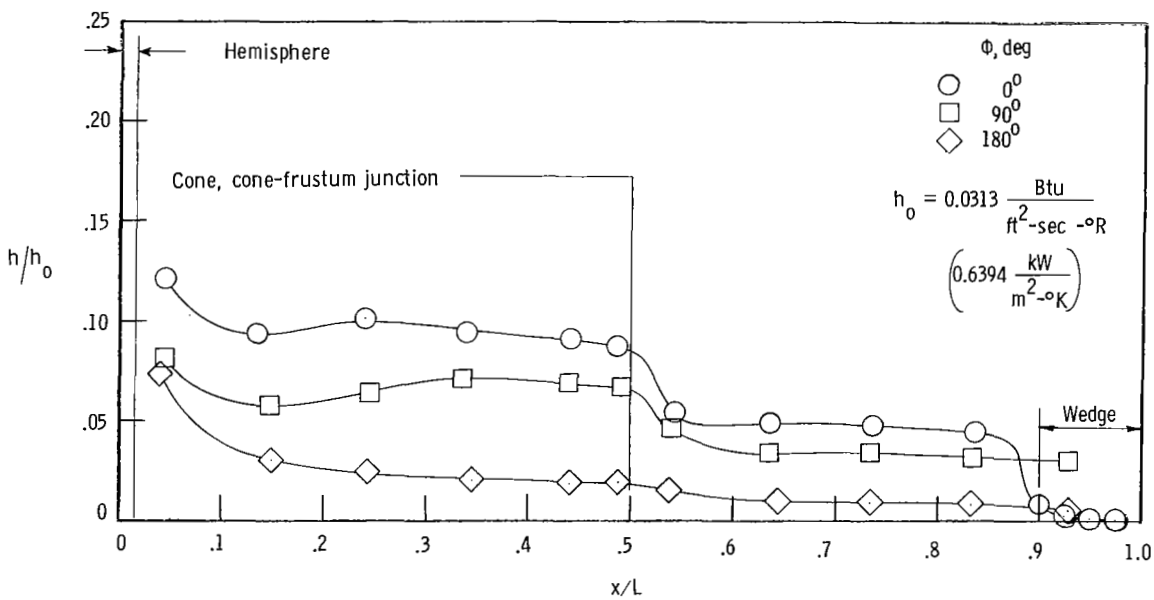

(b) Longitudinal distributions.

Figure 4.- Heat-transfer distributions for cone, cone-frustum configuration at $\alpha = 5^0$, $M_\infty = 10.23$, and $R_{\infty,L} = 1.47 \times 10^6$.

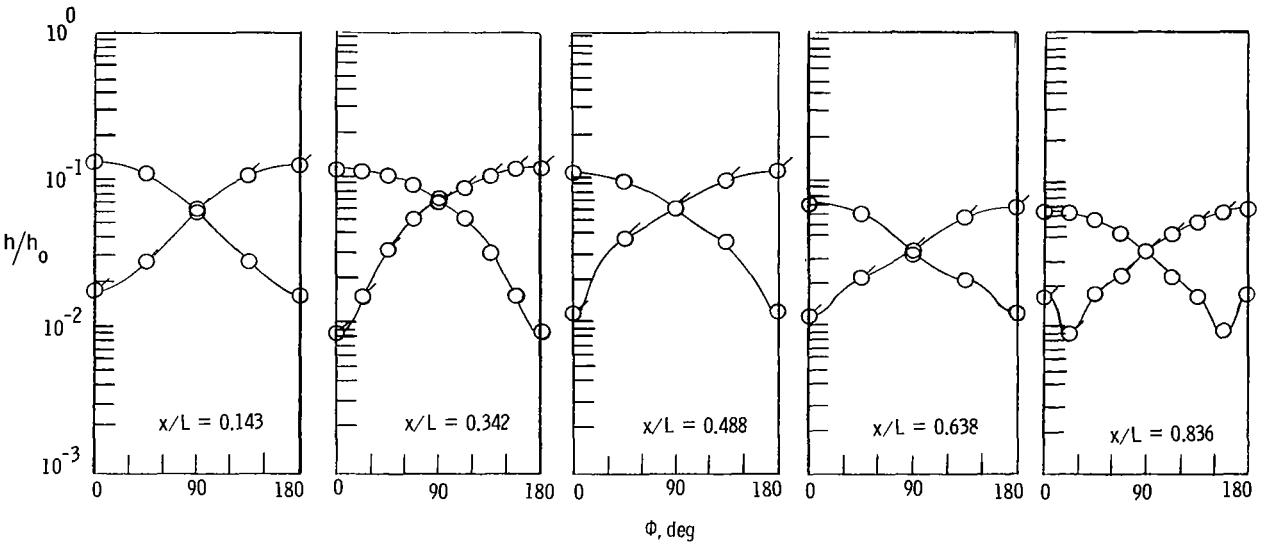

(a) Circumferential distributions.

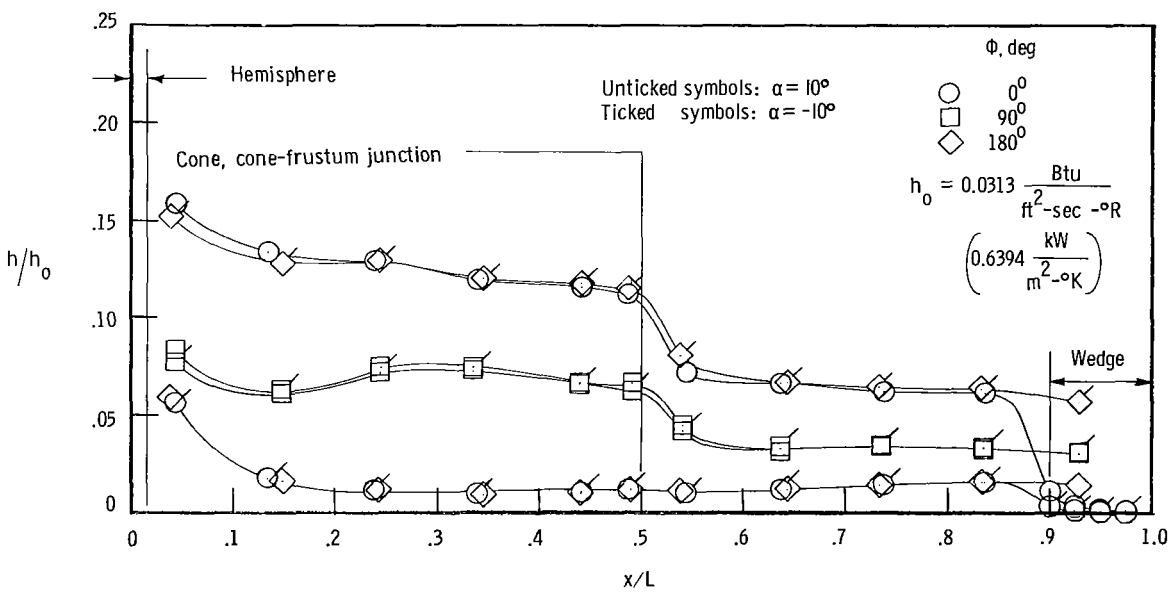

(b) Longitudinal distributions.

Figure 5.- Heat-transfer distributions for cone, cone-frustum configuration at $\alpha = \pm 10^0$, $M_\infty = 10.23$, and $R_{\infty,L} = 1.47 \times 10^6$.

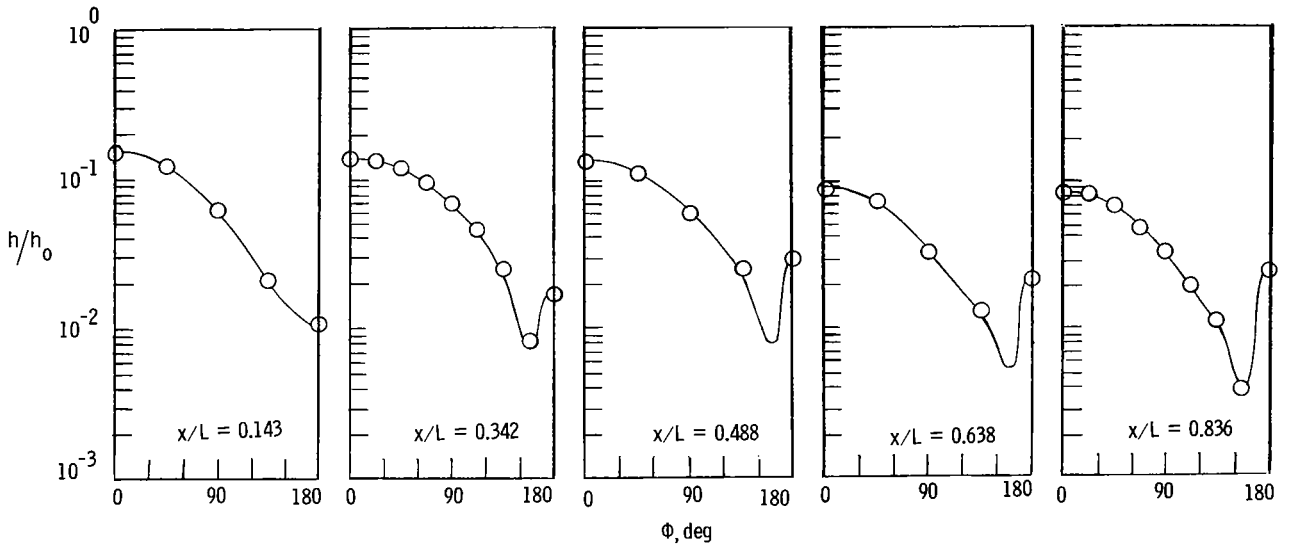

(a) Circumferential distributions.

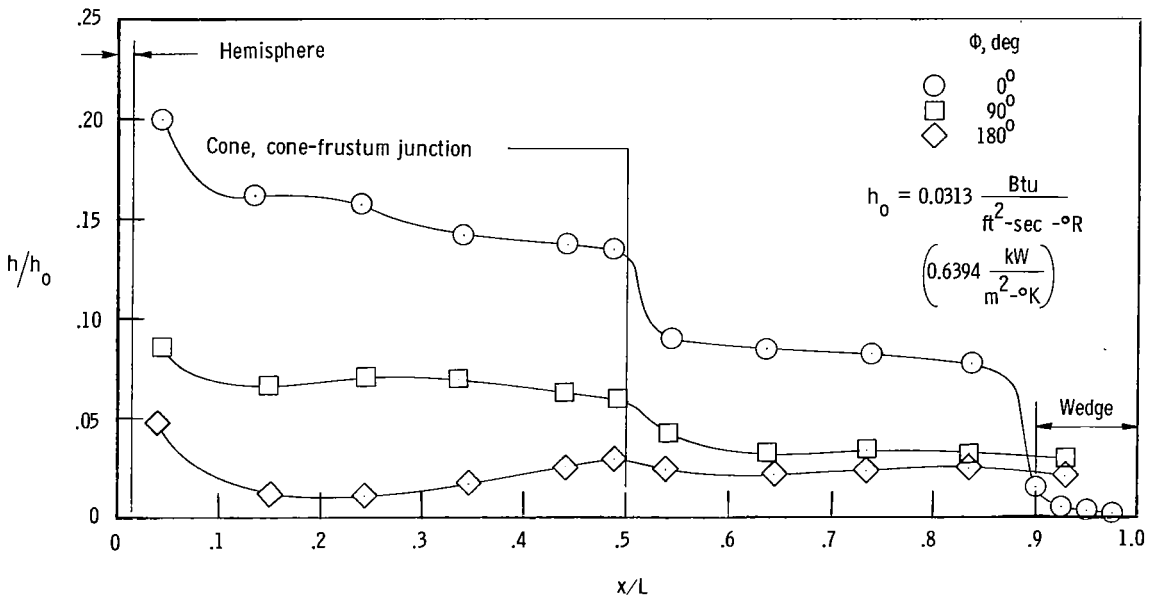

(b) Longitudinal distributions.

Figure 6.- Heat-transfer distributions for cone, cone-frustum configuration at $\alpha = 15^0$, $M_\infty = 10.23$, and $R_{\infty,L} = 1.47 \times 10^6$.

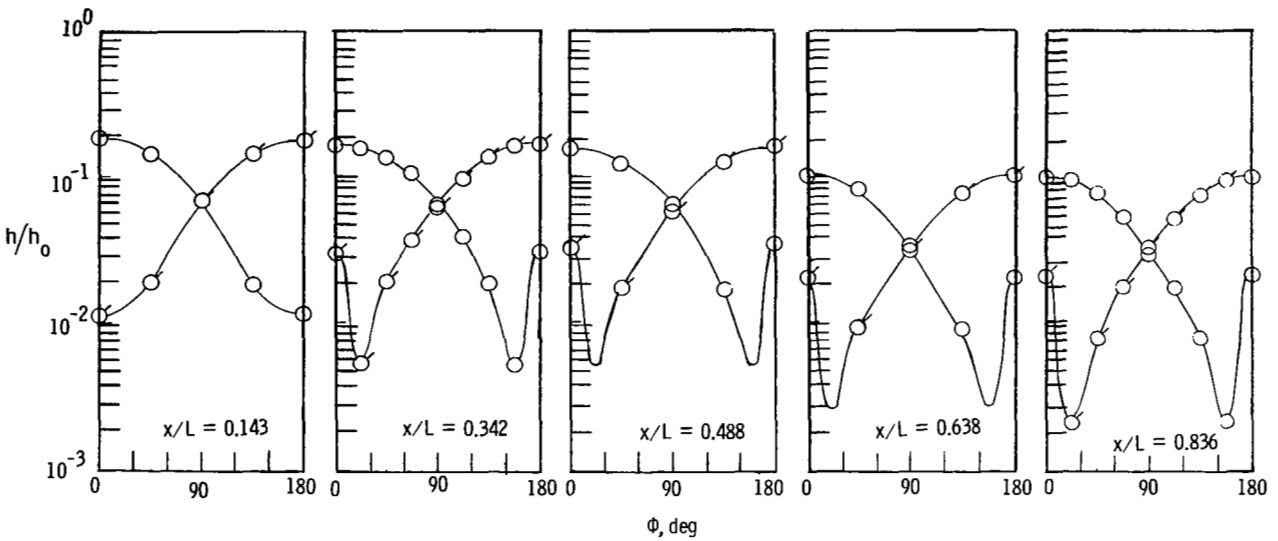

(a) Circumferential distributions.

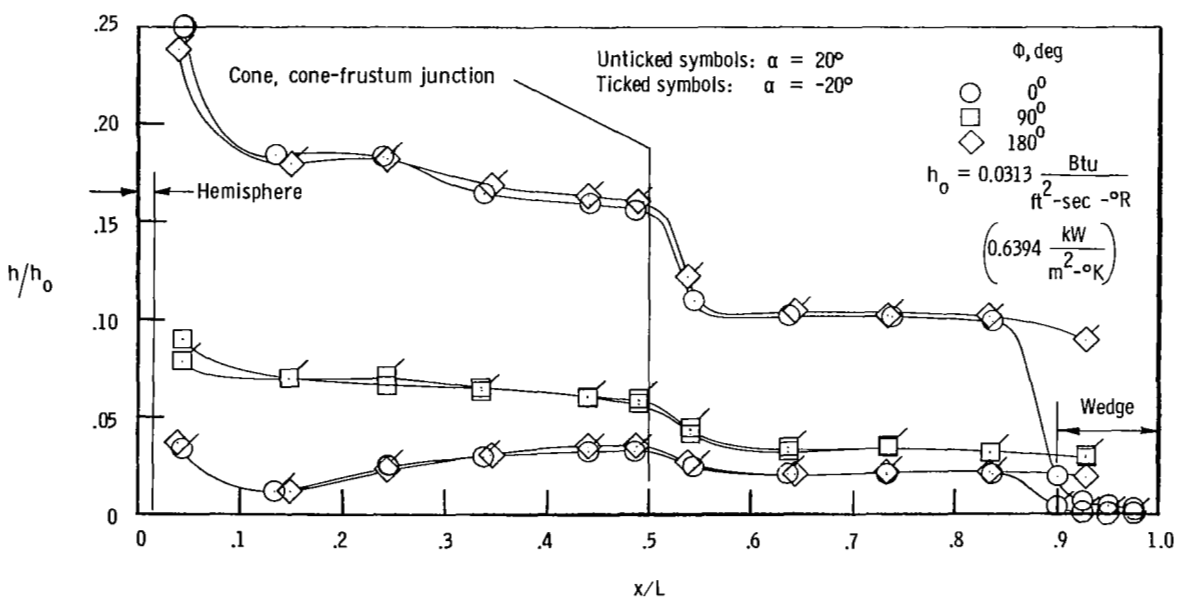

(b) Longitudinal distributions.

Figure 7.- Heat-transfer distributions for cone, cone-frustum configuration at $\alpha = \pm 20^0$, $M_\infty = 10.23$, and $R_{\infty,L} = 1.47 \times 10^6$.

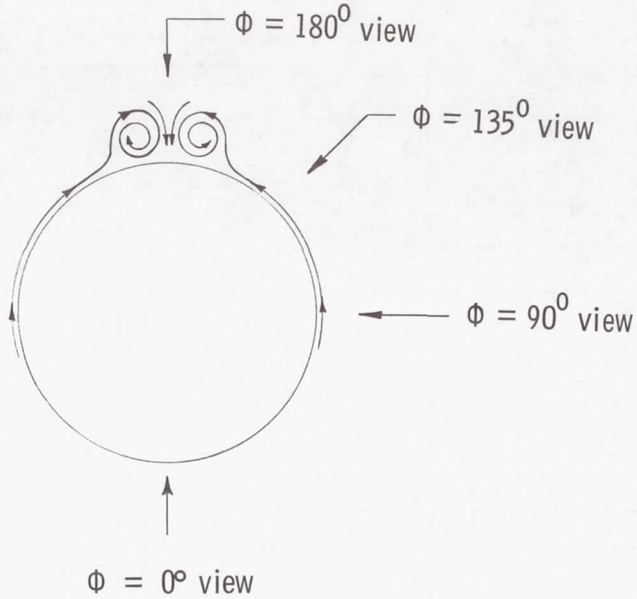

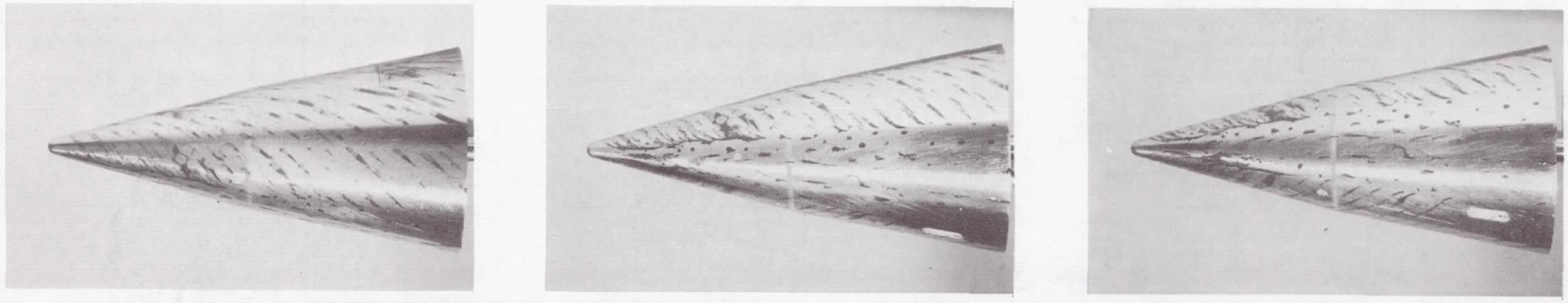

(a) $\Phi = 90^{\circ}$ view. (b) $\Phi = 135^{\circ}$ view. (c) $\Phi = 180^{\circ}$ view.

L-69-1228

Figure 8.- Flow patterns on the cone, cone-frustum model after 30 seconds at $M_{\infty} = 6.9$, $\alpha \cong 15^{\circ}$, and $R_{\infty,L} = 1.8 \times 10^{6}$.

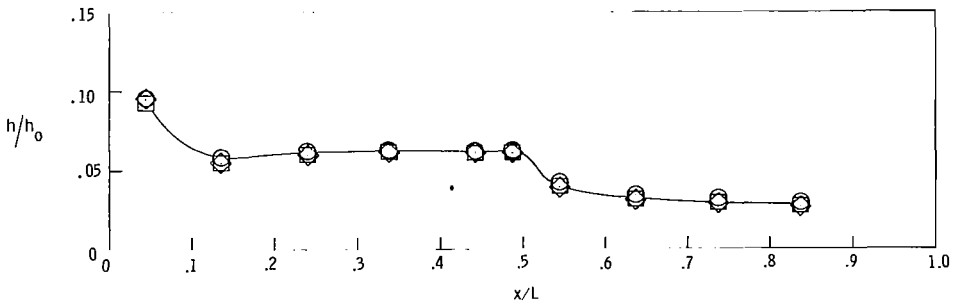

(a) $\alpha = 0^{\circ}$.

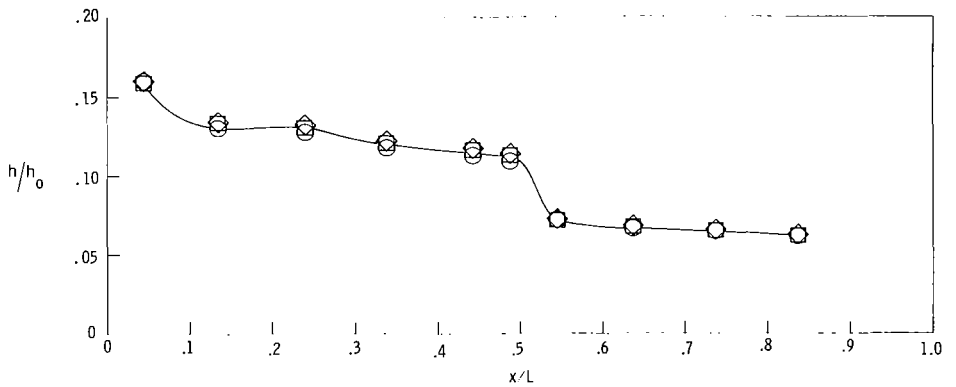

(b) $\alpha = 10^{\circ}$.

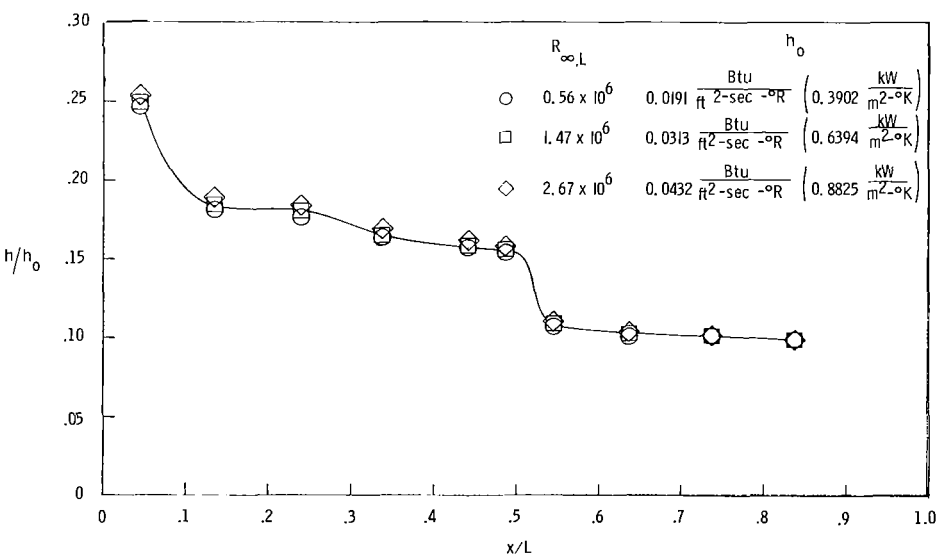

(c) $\alpha = 20^{\circ}$.

Figure 9.- Effect of Reynolds number and angle of attack on the windward-ray ($\Phi = 0^{\circ}$), longitudinal heating distributions.

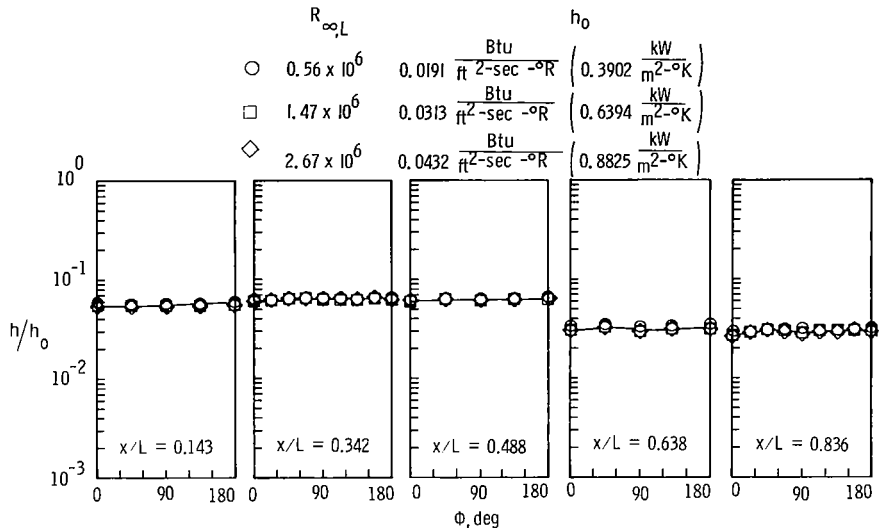

(a) α = 0°.

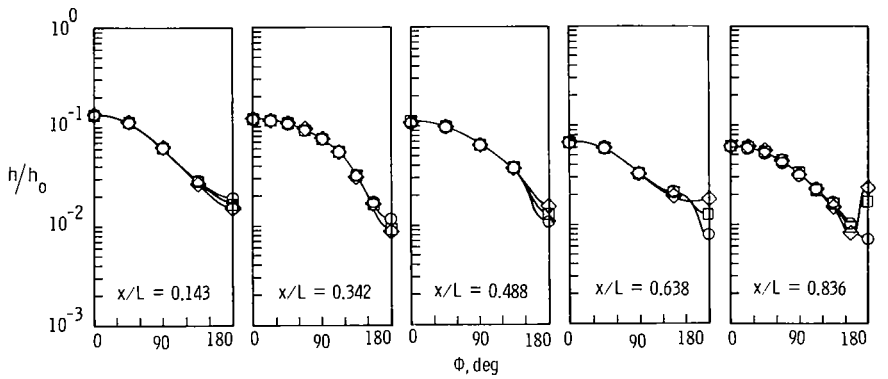

(b) α = 10°.

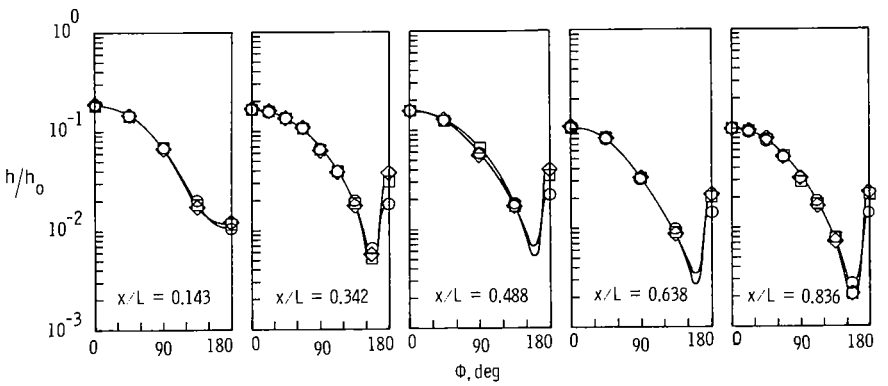

(c) α = 20°.

Figure 10.- Effect of Reynolds number and angle of attack on the circumferential heating distributions.

NASA-Langley, 1969 —— 33 L-6397